



Importance of El Niño reproducibility for reconstructing historical CO₂ flux variations in the equatorial Pacific

5 Michio Watanabe¹, Hiroaki Tatebe¹, Hiroshi Koyama¹, Tomohiro Hajima¹, Masahiro Watanabe², and Michio Kawamiya¹

¹Research Institute for Global Change, Japan Agency for Marine-Earth Science and Technology (JAMSTEC), 3173-25, Showa-machi, Kanazawa-ku, Yokohama, Kanagawa, 236-0001, Japan.

²Atmosphere and Ocean Research Institute, the University of Tokyo, 5-1-5, Kashiwanoha, Kashiwa, Chiba, 277-8564, Japan.

Correspondence to: Michio Watanabe (michiow@jamstec.go.jp)

10 **Abstract.** In the equatorial Pacific, air–sea CO₂ flux is known to fluctuate in response to inherent climate variability, predominantly the El Niño–Southern Oscillation (ENSO). For both investigation of the response of the carbon cycle to human-induced radiative perturbations and prediction of future global CO₂ concentrations, representation of the interannual fluctuation of CO₂ fluxes in Earth system models (ESMs) is essential. This study attempted to reproduce observed air–sea CO₂ flux fluctuations in the equatorial Pacific using two ESMs, to which observed ocean temperature and salinity data were
15 assimilated. When observations were assimilated into an ESM whose inherent ENSO variability was weaker than observations, nonnegligible correction terms on the governing equation of the equatorial ocean temperature caused anomalously false equatorial upwelling during El Niño periods that brought water rich in dissolved inorganic carbon from the subsurface layer to the surface layer. Contrary to observation, this resulted in an unusual upward air–sea CO₂ flux anomaly that should not occur during El Niño periods. The absence of such unrealistic upwelling anomalies in the other
20 ESM with the data assimilation reflects better representation of ENSO and the mean thermocline in this ESM without data assimilation. Our results demonstrate that adequate simulation of ENSO in an ESM is crucial for accurate reproduction of the variability in air–sea CO₂ flux and hence, in the carbon cycle.

1 Introduction

25 Since the industrial revolution, vast quantities of greenhouse gases (e.g., CO₂) have been released into the atmosphere through human activities such as fossil fuel use and land use change. Increased atmospheric CO₂ concentration leads to global warming; however, both the oceanic and the terrestrial ecosystems absorb atmospheric CO₂. Oceanic and terrestrial CO₂ uptake constitutes one of the major processes governing the fluctuation of the global carbon cycle (Sabine et al., 2004; Doney et al., 2009a, 2014; Le Quéré et al., 2009, 2010, 2016).



30 The goal of the Paris Agreement is to restrict the rise of the global mean surface temperature to well below 2 °C
relative to the preindustrial level. If greenhouse gas emissions continue to increase at their current rate, Earth's surface will
warm by 1.5 °C within ~20 years (Intergovernmental Panel on Climate Change (IPCC), 2018). In this context,
comprehensive understanding of the changes in the carbon cycle over previous years is essential for accurate prediction of
the carbon cycle, including natural fluctuations, which will assist in evaluation of future CO₂ emission reductions
35 (Kawamiya et al., 2019).

In the global climate, apart from the long-term warming trend associated with anthropogenic CO₂ emissions, there
are inherent, self-excited, internal climate variations with seasonal–decadal timescales, e.g., El Niño–Southern Oscillation
(ENSO), Pacific decadal variability, and Atlantic multidecadal variability. The solubility of CO₂ in the ocean is controlled
both by water properties such as temperature and salinity and by biogeochemical tracers, e.g., dissolved inorganic carbon
40 (DIC), transported by advection and diffusion. In addition, the air–sea CO₂ gas transfer velocity is a function of wind speed.
Therefore, fluctuation of the physical properties related to the internal climate variations strongly perturbs the air–sea CO₂
flux (hereafter, CO₂F, positive upward).

Observation-based studies have reached consensus that strong interannual variability of CO₂F exists in some
specific regions such as the equatorial Pacific and high latitudes of both hemispheres (e.g., Park et al., 2010; Valsala and
45 Maksyutov, 2010; Landschützer et al., 2014; Rödenbeck et al., 2014). The strong variation of CO₂F associated with ENSO
in the equatorial Pacific has been highlighted in many previous observation-based and simulation-based studies (Keeling and
Revelle, 1985; Feely et al., 1997, 1999; Jones et al., 2001; Obata and Kitamura, 2003; McKinley et al., 2004; Patra et al.,
2005). In the equatorial Pacific during El Niño periods (warm sea surface temperature), dissolved inorganic carbon (DIC)
concentration in the surface waters and CO₂F decrease because of reduced upwelling of cold DIC-rich deep water (Feely et
50 al., 2004; Doney et al., 2009a, 2009b). Le Borgne et al. (2002) estimated that upwelling of DIC-rich subsurface water
accounts for up to 70% of CO₂F variation in the equatorial Pacific, while the other 30% is attributable to the variation of
wind speed and biological processes. Accordingly, to estimate and predict fluctuations of CO₂ uptake by the global ocean on
timescales of several years, it would be informative to consider first the fluctuations in the equatorial Pacific associated with
ENSO.

55 Focusing on CO₂F fluctuations associated with ENSO in the equatorial Pacific, Dong et al. (2016) analyzed the
results of the Earth system models (ESMs) that participated in the Coupled Model Intercomparison Project (CMIP) Phase 5
(CMIP5; Taylor et al., 2012), which contributed to the Fifth Assessment Report (AR5) of the Intergovernmental Panel on
Climate Change (Intergovernmental Panel on Climate Change (IPCC), 2013). They showed that only some ESMs could
reproduce the observed anticorrelated relationship between sea surface temperature (SST) and CO₂F. For reliable prediction
60 of future CO₂ uptake on seasonal–decadal timescales, it would be preferable to employ an ESM capable of capturing this
anticorrelated relationship between SST and CO₂F.

For prediction of future physical states, previous studies used data assimilation systems to merge oceanic
observational and/or reanalysis data for initialization of a physical climate model to the current phase of the internal climate



65 variations. Variety of data assimilation techniques has been adopted, ranging from simple nudging technique (e.g., Behringer
et al., 1998; Ji et al., 1998; Smith et al., 2007; Keenlyside et al., 2008; Pohlmann et al., 2009; Sugiura et al., 2009; Mochizuki
et al., 2010; Tatebe et al., 2012) to more complex and computationally demanding techniques such as four-dimensional
variational method or ensemble Kalman filter (e.g., Kalman, 1960; Sasaki, 1969, 1970; Evensen, 1994; Hunt et al., 2004;
Kalnay et al., 2007; Yang et al., 2013). Furthermore, through incorporation into ESMs, the application of data assimilation
systems has been expanded to include biogeochemical properties, e.g., CO₂F monitoring, phytoplankton biomass monitoring,
70 and marine resource management (Brasseur et al., 2009; Tommasi et al., 2017a, 2017b; Park et al., 2018). Li et al. (2016,
2019) studied the predictability of CO₂F fluctuations of the global ocean by initializing ESMs with a data assimilation
system. However, they only compared the results of the initialized models with those of models with and without a data
assimilation system. The reproducibility of the observed anticorrelated relationship between SST and CO₂F associated with
ENSO, which is one of the most characteristic features in temporal global CO₂F variations, was not discussed
75 comprehensively.

In this study, as a first step toward predicting fluctuations in atmospheric CO₂ concentration, we assimilated
observed ocean data into two ESMs and evaluated historical fluctuations of CO₂F in the equatorial Pacific. One ESM had a
physical core where the ENSO amplitude is about half the observed value, whereas the other improved ESM showed ENSO
variation that is more realistic (Watanabe et al., 2010; Watanabe, M. et al., 2011). In this study, nudging technique is
80 employed. The technique is relatively simple compared to more elaborate ones such as ensemble Kalman filter and four-
dimensional variational method, but is widely used for decadal prediction of physical (Keenlyside et al., 2008; Pohlmann et
al., 2009; Mochizuki et al., 2010; Tatebe et al., 2012) and biogeochemical (Li et al., 2016, 2019; Sospedra-Alfonso and Boer,
2020) states. Positive aspects of nudging technique include its readiness to examine the effects of introducing data
assimilation on physical processes. Through comparison of the results produced by the two ESMs both with and without the
85 data assimilation, we clarified the key to accurate reproduction of the CO₂F fluctuations associated with ENSO. However,
spatiotemporal observations of DIC concentration are insufficient for use in the assimilation; therefore, this study used ocean
physical objective analysis data. This remainder of this paper is organized as follows. Sect. 2 provides a brief description of
the models used in this study, and the derived results are presented in Sect. 3. Finally, a short discussion and a summary are
presented in Sect. 4.

90

2 Methods

2.1 Model Description

This study used two ESMs, i.e., the MIROC-ESM, referred to hereafter as OLD (Watanabe, S. et al., 2011) and the
MIROC-ES2L, referred to hereafter as NEW (Hajima et al., 2020). The former is an official model of CMIP5, while the
95 latter is newly developed for CMIP Phase 6 (CMIP6; Eyring et al., 2016). The physical core model of OLD is MIROC3m,



while that of NEW is MIROC5.2, which represents a minor update of MIROC5 by Watanabe, M. et al. (2010; 2011). The horizontal resolution of the atmospheric component of OLD (NEW) has T42 spectral truncation (i.e., approximately 300 km) with 80 (40) vertical levels up to 0.003 hPa (3 hPa). In OLD, the longitudinal grid spacing of the oceanic component is approximately 1.4°, while the latitudinal grid intervals vary gradually from 0.5° at the equator to 1.7° near both poles. There are 44 vertical levels, the lowermost of which is located at the depth of 5300 m. The oceanic component of NEW has a horizontal tripolar coordinate system. In the spherical coordinate portion south of 63°N, the longitudinal grid spacing is 1°, while the meridional grid spacing varies from approximately 0.5° near the equator to 1° in mid-latitude regions. There are 63 vertical levels, the lowermost of which is located at the depth of 6300 m.

In this study, embedded in both ESMs was the same simple scheme for ocean data assimilation, which comprised an incremental analysis update (IAU; Bloom et al., 1996; Huang et al., 2002). In the IAU, during the analysis interval from $t = 0$ to $t = \tau$, the governing equation including a correction term for temperature and salinity (X) is written as follows:

$$\frac{dX}{dt} = \text{adv.} + \text{diff.} + F + \frac{\alpha}{\tau} \Delta X^{\alpha}, \quad (1)$$

where adv. is the advection term, diff. is the diffusion term, F is the surface flux term, and the final term on the right-hand side is the correction term with α as a constant, and ΔX^{α} as the analysis increment. The analysis increment is calculated from $\Delta X^{\alpha} = X^{\alpha}(0) - X(0)$, where $X^{\alpha}(0)$ is the analysis and $X(0)$ is the model first guess at $t = 0$; this term is held constant during the analysis interval. Following Tatebe et al. (2012), we employed values of $\tau = 1$ d and $\alpha = 0.025$. The monthly objective analysis data of ocean temperature and salinity (Ishii and Kimoto, 2009) were interpolated linearly to form daily analysis data, X^{α} . Hereafter, the OLD (NEW) model embedded with the IAU scheme is called OLD-assim (NEW-assim).

OLD and NEW were integrated for spinup under preindustrial forcing until reaching an equilibrium state. Then, a set of historical runs with external forcing based on observations from 1850 through to 2005 (i.e., the end year of the historical run in CMIP5) was conducted. Note that OLD and OLD-assim (NEW and NEW-assim) were driven with CMIP5 (CMIP6) forcing. Data assimilation started at 1946 to reflect the time span of observed ocean data. The model results from 1961–2005 were used for analysis. There were three ensemble members for each run of OLD/NEW and OLD/NEW-assim.

2.2 Estimating pCO₂ change at the sea surface

CO₂F depends on the difference in CO₂ partial pressure between the sea and the air, i.e.:

$$\text{CO}_2\text{F} = K(\text{pCO}_2 - \text{pCO}_2^{\text{air}})(1 - \gamma), \quad (2)$$

where pCO_2 ($\text{pCO}_2^{\text{air}}$) is the CO₂ partial pressure in the sea (air), γ is the fraction of sea ice, and $K = k\alpha$ is the CO₂ gas transfer coefficient, where k represents the CO₂ gas transfer velocity (Wanninkhof, 1992, 2014) and α represents the solubility of CO₂ in seawater (Weiss, 1974). The CO₂ gas transfer velocity k is a function of wind speed and the Schmidt number (Wanninkhof, 1992). This study investigated the reproducibility of the anticorrelated relationship between CO₂F and SST and therefore the direction of the flux is important. As K does not affect the direction and the flux variation due to



ENSO has larger amplitude in terms of $p\text{CO}_2$ than $p\text{CO}_2^{\text{air}}$ (Dong et al., 2017), the direction of flux is governed by the variation in $p\text{CO}_2$. Consequently, we evaluated the $p\text{CO}_2$ change at the sea surface in the equatorial Pacific.

130 Seawater $p\text{CO}_2$ values depend on temperature (T), salinity (S), DIC concentration, and total alkalinity (Alk); therefore, the change of $p\text{CO}_2$ can be expanded as follows:

$$\Delta p\text{CO}_2 = \frac{\partial p\text{CO}_2}{\partial T} \Delta T + \frac{\partial p\text{CO}_2}{\partial S} \Delta S + \frac{\partial p\text{CO}_2}{\partial \text{DIC}} \Delta \text{DIC} + \frac{\partial p\text{CO}_2}{\partial \text{Alk}} \Delta \text{Alk} + \text{Res.}, \quad (3)$$

where Res., which includes second-order terms (Takahashi et al., 1993), was estimated as $\Delta p\text{CO}_2 - (\partial p\text{CO}_2/\partial T)\Delta T - (\partial p\text{CO}_2/\partial S)\Delta S - (\partial p\text{CO}_2/\partial \text{DIC})\Delta \text{DIC} - (\partial p\text{CO}_2/\partial \text{Alk})\Delta \text{Alk}$ in this study. In Sect. 3, we first evaluate the CO_2F and $p\text{CO}_2$ 135 fluctuations in the equatorial Pacific in both NEW-assim and OLD-assim, and we calculate each term in Eq. (3) for each model.

3 Results

3.1 CO_2 flux and $p\text{CO}_2$ anomaly in Niño3 region

140 The time variations in the Niño3 region (5°S – 5°N , 90° – 150°W) of both SST (hereafter, NINO3-SST) and CO_2F (hereafter, NINO3- CO_2F) simulated with OLD-assim (NEW-assim) are shown in Figure 1a (Figure 1b). The correlation coefficient between NINO3-SST and NINO3- CO_2F in NEW-assim (OLD-assim) is -0.41 (0.44). It suggests that the observed anticorrelated relationship is captured well in NEW-assim but not in OLD-assim. Dong et al. (2016) showed that OLD could capture the observed anticorrelated relationship between SST and CO_2F in the equatorial Pacific; however, 145 OLD-assim could not reproduce this relationship.

As the direction of CO_2F is determined mainly by $p\text{CO}_2$ at the sea surface (see Eq. (2)), we further estimated each term in Eq. (3) for each model output (Figure 2). We estimated ΔX ($X = p\text{CO}_2$, T, S, DIC, or Alk) in Eq. (3) as X regressed on the NINO3-SST averaged over the entire Niño3 region, while $\partial p\text{CO}_2/\partial X$ was estimated based on the climatological annual mean T, S, DIC, and Alk at the sea surface within the Niño3 region in each model. In OLD, the impact of the change 150 in DIC concentration (i.e., the absolute value of $(\partial p\text{CO}_2/\partial \text{DIC})\Delta \text{DIC}$) is larger than that of the change in CO_2 solubility due to temperature increase (i.e., $(\partial p\text{CO}_2/\partial T)\Delta T$) and thus $\Delta p\text{CO}_2$ becomes negative during El Niño periods. However, in OLD-assim, $(\partial p\text{CO}_2/\partial T)\Delta T$ is larger than in OLD and the absolute value of $(\partial p\text{CO}_2/\partial \text{DIC})\Delta \text{DIC}$ is smaller, resulting in positive $\Delta p\text{CO}_2$ during El Niño periods. In NEW and NEW-assim, the absolute value of $(\partial p\text{CO}_2/\partial \text{DIC})\Delta \text{DIC}$ is large, causing negative $\Delta p\text{CO}_2$. As noted in Sect. 1, previous studies (Le Borgne et al., 2002; Feely et al., 2004; Doney et al., 2009a, 155 2009b) showed that variability in upwelling during ENSO events dominates equatorial Pacific CO_2F through its regulation of DIC. In the following, we discuss the temperature and upwelling velocity changes during El Niño periods along the Equator.



3.2 DIC and upwelling changes in OLD and OLD-assim

160 Here, we analyze the model results of both OLD-assim and OLD. A cross section of the monthly ocean
temperature anomaly regressed onto NINO3-SST along the Equator within the Pacific is presented in Figure 3, together with
the climatological annual mean depths of the 18, 20, and 22 °C isotherms. Here, monthly temperature anomalies were
calculated with respect to the 1971–2000 monthly mean climatology. In comparison with observations (Figure 3c) (Ishii and
Kimoto, 2009), the climatological mean state of OLD shows an equatorial thermocline that is more diffuse than observed. In
165 addition, the temperature increase during El Niño periods in OLD is smaller (Figure 3a). The standard deviation of NINO3-
SST in OLD was calculated as 0.43 °C, i.e., approximately half that derived from the COBESST2 dataset (0.71 °C) (Ishii et
al., 2005; Hirahara et al., 2014). Our result is consistent with Meehl et al. (2001), who reported that a climate model with a
climatological mean state of a diffuse equatorial thermocline showed a smaller increase in SST during El Niño periods. The
process of strengthening or weakening of the upwelling that passes through the thermocline is important for SST fluctuations
170 associated with ENSO. When the thermocline is diffuse, the temperature difference between the top and bottom of the
thermocline is reduced, and the effect of the upwelling passing through the thermocline on SST fluctuation is diminished.

We estimated the strength of this feedback in OLD. For this purpose, we evaluated the westerly wind anomaly in
the equatorial central Pacific as the zonal wind anomaly at 10 m height above the sea surface within the Niño4 region (5°S–
5°N, 160°E–150°W) (hereafter, NINO4-U10) (Guilyardi et al., 2009). Similarly, we calculated the vertical velocity at the
175 depth of the oceanic thermocline (often measured by the depth of the 20 °C isotherm (e.g., Lengaigne et al., 2012; Li and Xie,
2014)) averaged over the Niño3 region (hereafter, NINO3-WO). Then, the wind feedback (vertical velocity feedback) was
computed as the regression of NINO4-U10 over NINO3-SST ($\text{m s}^{-1} \text{ } ^\circ\text{C}^{-1}$) (regression of NINO3-WO over NINO3-SST (m
 $\text{s}^{-1} \text{ } ^\circ\text{C}^{-1}$)). The black cross in Figure 4 shows the strength of the wind and vertical velocity feedbacks evaluated from OLD.
The wind (vertical velocity) feedback of $0.46 \text{ m s}^{-1} \text{ } ^\circ\text{C}^{-1}$ ($-0.49 \times 10^{-6} \text{ m s}^{-1} \text{ } ^\circ\text{C}^{-1}$) indicates positive feedback (an enhanced
180 warm SST anomaly). However, this wind feedback is less than half that evaluated from the JRA55 reanalysis wind dataset
(Kobayashi et al., 2015) and the COBESST2 dataset (Ishii et al., 2005; Hirahara et al., 2014), i.e., $1.02 \text{ m s}^{-1} \text{ } ^\circ\text{C}^{-1}$ (thin
dashed line in Figure 4).

Cross sections of the monthly upward water velocity and DIC concentration anomalies along the Equator regressed
onto NINO3-SST in OLD without assimilation are shown in Figure 5a and 5b, respectively. The weak ENSO signal in the
185 zonal wind in OLD (Figure 4) leads to a decrease in water upwelling of just 10^{-6} m s^{-1} in the equatorial Pacific (Figure 5a).
Although the ENSO signal in OLD (without assimilation) is weak because of weakened upwelling of subsurface DIC-rich
waters (Figure 5a), the DIC concentration of the surface waters decreases (Figure 5b). This is consistent with Dong et al.
(2016), showing that OLD is able to reproduce qualitatively the anticorrelated relationship between temperature and DIC
concentration.

190 We investigated the correction in temperature due to the data assimilation (temperature increment, the final term
on the right-hand side of Eq. (1)) and the fluctuations in vertical velocity and DIC concentration in OLD-assim. The monthly



mean temperature increment, vertical velocity, and DIC concentration along the Equator regressed onto NINO3-SST are shown in Figure 6a–c, respectively. As the temperature increase during El Niño periods in OLD is smaller than observed (Figure 3a and 3c), data assimilation causes the water temperature to increase by $0.16 \times 10^{-6} \text{ }^\circ\text{C s}^{-1}$ at the depth of the thermocline (the depth of the $20 \text{ }^\circ\text{C}$ isotherm) in the eastern equatorial Pacific (Figure 6a). The wind feedback in OLD-assim is $0.49 \text{ m s}^{-1} \text{ }^\circ\text{C}^{-1}$ (red cross in Figure 4), which is the same as in OLD; however, the strong heating causes upwelling of DIC-rich waters in the subsurface layers (Figure 6b). The positive value of vertical velocity feedback in Figure 4 indicates enhancement of subsurface cold water upwelling and weakening of the SST increase. This unrealistically prevents El Niño from developing fully. This upwelling also causes the DIC concentration in the surface layer to increase (Figure 6c), leading to positive correlation between SST and CO₂F (Figure 1b), contrary to observations.

3.3 DIC change in NEW and NEW-assim

Here, we analyze the model results of NEW and NEW-assim, which capture the observed anticorrelated relationship between NINO3-SST and NINO3-CO₂F (Figure 1b).

A cross section of the monthly mean water temperature regressed onto NINO3-SST along the Equator in NEW is shown in Figure 3b. Compared with OLD (Figure 3a), a stronger fluctuation of water temperature is observed in NEW. The standard deviation of NINO3-SST is $1.14 \text{ }^\circ\text{C}$. Note that this value is larger than both that in OLD ($0.43 \text{ }^\circ\text{C}$) and that derived from the COBESST2 dataset ($0.71 \text{ }^\circ\text{C}$).

As mentioned in Sect. 3.2, El Niño is associated with both a westerly wind anomaly in the central equatorial Pacific and a vertical velocity anomaly in the eastern equatorial Pacific. The wind feedback in NEW of $0.90 \text{ m s}^{-1} \text{ }^\circ\text{C}^{-1}$ (black circle in Figure 4) is much larger than in OLD ($0.46 \text{ m s}^{-1} \text{ }^\circ\text{C}^{-1}$). We also note that this is comparable with that evaluated from the JRA55 reanalysis (Kobayashi et al., 2015), i.e., $1.02 \text{ m s}^{-1} \text{ }^\circ\text{C}^{-1}$. Thus, based on the fluctuations in water temperature and wind speed, it can be said that ENSO reproducibility in NEW is better than in OLD.

A cross section of the monthly vertical velocity anomaly regressed onto NINO3-SST in NEW is shown in Figure 7a. The stronger ENSO signal in the zonal wind in NEW in comparison with OLD causes greater decrease in upwelling of approximately $5 \times 10^{-6} \text{ m s}^{-1}$. The vertical velocity feedback is estimated as $-0.47 \times 10^{-6} \text{ m s}^{-1} \text{ }^\circ\text{C}^{-1}$ (black circle in Figure 4). A cross section of the monthly DIC concentration anomaly regressed onto NINO3-SST is shown in Figure 7b. Owing to the westerly wind anomaly and the decrease in upwelling, NEW is able to reproduce the realistic decrease in DIC concentration during El Niño periods.

Here, we investigate the model results of NEW-assim. The monthly temperature increment, vertical velocity, and DIC concentration anomalies along the Equator regressed onto NINO3-SST in NEW-assim are shown in Figure 8a–c, respectively. The large absolute value of the temperature increment is found only in surface layers with temperatures $>22 \text{ }^\circ\text{C}$, whereas that in the thermocline between the isotherms of 18 and $22 \text{ }^\circ\text{C}$ is merely $0.06 \times 10^{-6} \text{ }^\circ\text{C s}^{-1}$ (Figure 8a), i.e., much smaller than in OLD-assim ($0.16 \times 10^{-6} \text{ }^\circ\text{C s}^{-1}$; Figure 6a). In NEW-assim, the wind feedback of $0.93 \text{ m s}^{-1} \text{ }^\circ\text{C}^{-1}$ (red circle



225 in Figure 4) is of similar magnitude to that in NEW ($0.90 \text{ m s}^{-1} \text{ }^{\circ}\text{C}^{-1}$). The westerly wind anomaly in NEW-assim leads to
decrease in upwelling of subsurface waters along the Equator (Figure 8b), and the vertical velocity feedback of -0.47×10^{-6}
 $\text{m s}^{-1} \text{ }^{\circ}\text{C}^{-1}$ is again of similar magnitude to that in NEW. The finding that the wind and vertical velocity feedbacks in NEW-
assim act in a manner consistent with NEW indicates that ocean data assimilation does not cause spurious
upwelling/downwelling in NEW-assim. The diminished upwelling in NEW-assim leads to decrease in the DIC concentration
230 (Figure 8c), resulting in the anticorrelated relationship between SST and DIC concentration.

4 Discussion and Summary

The equatorial Pacific is the region where most prominent interannual variability of CO₂F can be seen (e.g., Park
et al., 2010; Valsala and Maksyutov, 2010; Landschützer et al., 2014; Rödenbeck et al., 2014). In this research, the same
235 simple data assimilation scheme is incorporated into two ESMs, OLD in which the ENSO amplitude is about half the
observed value and NEW with improved reproducibility of ENSO. The correlation between SST and CO₂F in the equatorial
Pacific is consistently represented only in the case where the ocean temperature and salinity observations are assimilated into
NEW. Response of the equatorial trade wind to the observed SST was significantly weaker than observed in OLD with the
data assimilation, which cannot support the development of the equatorial subsurface temperature variations during El Niño
240 periods with comparable amplitude in observations. Instead, relative importance of the correction term on the governing
equation of the ocean temperature, which is introduced in the data assimilation procedure, becomes nonnegligible, and
advection-diffusion balance of the temperature is biased with respect to model's physical nature. Resultant spurious
equatorial upwelling of subsurface DIC-rich water to the surface layer works to increase the surface DIC concentration
during El Niño periods, and thus, unrealistic upward CO₂F occurs in the case where the data assimilation is incorporated
245 into OLD. We conclude that faithful representation of the processes in the equatorial climate system is crucial for improved
initialization and subsequent prediction in marine ecosystem modeling.

Focusing on the CO₂F fluctuations associated with ENSO in the equatorial Pacific, Dong et al. (2016) analyzed
the results of the CMIP5 ESMs. They showed that only a portion of CMIP5 ESMs (including OLD) could reproduce the
observed anticorrelated relationship between SST and CO₂F. Bellenger et al. (2014) evaluated the reproducibility of ENSO
250 in the CMIP5 models. They reported that most CMIP5 climate models and ESMs underestimate the amplitude of the wind
stress feedback by 20%–50%, and that only 20% of CMIP5 models have relative error within 25% of the observed value.
Our study indicated that reliable future prediction of CO₂F in the equatorial Pacific would benefit from faithful reproduction
of wind feedback in ESMs that is sufficiently strong to capture the anticorrelated relationship between SST and CO₂F, even
with data assimilation.

255 In this study, as a first step toward predicting fluctuations in atmospheric CO₂ concentration, we discussed
fluctuations in CO₂F attributable directly to ENSO. It is also known that CO₂F fluctuates in association with Pacific decadal



variability (Valsala et al., 2012) and Atlantic multidecadal variability (Breedeen and McKinley, 2016). In addition, land–air CO₂ flux also fluctuates in association with ENSO (Eldering et al., 2017). The reproducibility of fluctuations in CO₂F in other regions as well as those of land–air CO₂ flux remains a topic for future research.

260

Data availability

The CMIP5 forcing data is described at <https://pcmdi.llnl.gov/mips/cmip5/forcing.html> and the CMIP6 forcing data is version 6.2.1. The JRA55 reanalysis wind dataset is available at https://jra.kishou.go.jp/JRA-55/index_en.html. The COBESST2 dataset is available at <https://www.esrl.noaa.gov/psd/data/gridded/data.cobe2.html>. The postprocessing scripts used for this research and the data used in the figures can be obtained online (<https://osf.io/mpk52>).

265

Author contribution

MiW, HT, MaW, and MK contributed to the experiment design. MiW and HK embedded the ocean data assimilation system into the ESMs. MiW and TH performed the experimental simulations. MiW analyzed the model output and drafted the paper. All authors discussed the results, and commented on and edited the manuscript.

270

Competing interests

The authors declare that they have no conflict of interest.

275 Acknowledgments

This work was supported by the Integrated Research Program for Advanced Climate Models (TOUGOU) Grant Numbers JPMXD0717935457 and JPMXD0717935715 from the Ministry of Education, Culture, Sports, Science and Technology, MEXT, Japan.

280



References

- Behringer, D. W., Ji, M., and Leetmaa, A.: An improved coupled model for ENSO prediction and implications for ocean initialization. Part I: The ocean data assimilation system, *Mon. Weather Rev.*, 126, 1013–1021, doi:10.1175/1520-0493(1998)126<1013:AICMFE>2.0.CO;2, 1998
- 285
- Bellenger, H., Guilyardi, E., Leloup, J., Lengaigne, M., and Vialard, J.: ENSO representation in climate models: From CMIP3 to CMIP5, *Clim. Dyn.*, 42, 1999–2018, doi:10.1007/s00382-013-1783-z, 2014.
- Bloom, S. C., Takacs, L. L., da Silva, A. M., and Ledvina, D.: Data assimilation using incremental analysis updates, *Mon. Weather Rev.*, 124, 1256–1271, 1996.
- 290
- Brasseur, P., Gruber, N., Barciela, R., Brander, K., Doron, M., El Moussaoui, A., Hobday, A. J., Huret, M., Kremer, A.-S., Lehodey, P., Matear, R., Moulin, C., Murtugudde, R., Senina, I., and Svendsen, E.: Integrating biogeochemistry and ecology into ocean data assimilation systems, *Oceanography*, 22(3), 206–215, doi:10.5670/oceanog.2009.80, 2009.
- Breeden, M. L., and McKinley, G. A.: Climate impacts on multidecadal pCO₂ variability in the North Atlantic: 1948–2009, *Biogeosciences*, 13, 3387–3396, doi:10.5194/bg-13-3387-2016, 2016.
- 295
- Doney, S. C., Bopp, L., and Long, M. C.: Historical and future trends in ocean climate and biogeochemistry, *Oceanography*, 27(1), 108–119, doi:10.5670/oceanog.2014.14, 2014.
- Doney, S. C., Balch, W. M., Fabry, V. J., and Feely, R. A.: Ocean acidification: A critical emerging problem for the ocean sciences, *Oceanography*, 22(4), 16–25, doi:10.5670/oceanog.2009.93, 2009a.
- Doney, S. C., Fabry, V. J., Feely, R. A., and Kleypas, J. A.: Ocean acidification: The other CO₂ problem, *Annu. Rev. Mar. Sci.*, 1, 169–192, doi:10.1146/annurev.marine.010908.163834, 2009b.
- 300
- Dong, F., Li, Y., Wang, B., Huang, W., Shi, Y., and Dong, W.: Global air–sea CO₂ flux in 22 CMIP5 models: Multiyear mean and interannual variability, *J. Clim.*, 29, 2407–2431, doi:10.1175/JCLI-D-14-00788.1, 2016.
- Dong, F., Li, Y., and Wang, B.: Assessment of responses of Tropical Pacific air–sea CO₂ flux to ENSO in 14 CMIP5 models, *J. Clim.*, 30, 8595–8613, doi:10.1175/JCLI-D-16-0543.1, 2017.
- 305
- Eldering, A., Wennberg, P. O., Crisp, D., Schimel, D. S., Gunson, M. R., Chatterjee, A., Liu, J., Schwandner, F. M., Sun, Y., O’Dell, C. W., Frankenberg, C., Taylor, T., Fisher, B., Osterman, G. B., Wunch, D., Hakkarainen, J., Tamminen, J., and Weir, B.: The Orbiting Carbon Observatory-2 early science investigations of regional carbon dioxide fluxes, *Science*, 358, eaam5745, doi:10.1126/science.aam5745, 2017.
- Evensen, G.: Sequential data assimilation with a nonlinear quasi-geostrophic model using Monte Carlo methods to forecast error statistics, *J. Geophys. Res.*, 99, 10143–10162. 1994.
- 310
- Eyring, V., Bony, S., Meehl, G. A., Senior, C. A., Stevens, B., Stouffer, R. J., and Taylor, K. E.: Overview of the Coupled Model Intercomparison Project Phase 6 (CMIP6) experimental design and organization, *Geosci. Model Dev.*, 9, 1937–1958, doi:10.5194/gmd-9-1937-2016, 2016.



- 315 Feely, R. A., Wanninkhof, R., Goyet, C., Archer, D. E., and Takahashi, T.: Variability of CO₂ distributions and sea–air fluxes in the central and eastern equatorial Pacific during the 1991–1994 El Niño, *Deep-Sea Res. II*, 44, 1851–1867, doi:10.1016/S0967-0645(97)00061-1, 1997.
- Feely, R. A., Wanninkhof, R., Takahashi, T., and Tans, P.: Influence of El Niño on the equatorial Pacific contribution to atmospheric CO₂ accumulation, *Nature*, 398, 597–601, doi:10.1038/19273, 1999.
- 320 Feely, R. A., Wanninkhof, R., McGillis, W., Carr, M.-E., and Cosca, C. E.: Effects of wind speed and gas exchange parameterizations on the air–sea CO₂ fluxes in the equatorial Pacific Ocean, *J. Geophys. Res.*, 109, C08S03, doi:10.1029/2003JC001896, 2004.
- Guilyardi, E, Braconnot, P., Jin, F.-F., Kim, S. T., Koliasinski, M., Li, T., and Musat, I.: Atmosphere feedbacks during ENSO in a coupled GCM with a modified atmospheric convection scheme, *J. Clim.*, 22, 5698–5718, doi:10.1175/2009JCLI2815.1, 2009.
- 325 Hajima, T., Watanabe, M., Yamamoto, A., Tatebe, H., Noguchi, M. A., Abe, M., Ohgaito, R., Ito, A., Yamazaki, D., Okajima, H., Ito, A., Takata, K., Ogochi, K., Watanabe, S., and Kawamiya, M.: Description of the MIROC-ES2L Earth system model and evaluation of its climate–biogeochemical processes and feedback, *Geosci. Model Dev.*, doi:10.5194/gmd-2019-275, accepted, 2020.
- 330 Hirahara, S., Ishii, M., and Fukuda, Y.: Centennial-scale sea surface temperature analysis and its uncertainty, *J. Clim.*, 27, 55–75, doi:10.1175/JCLI-D-12-00837.1, 2014.
- Huang, B., Kinter, J. L., and Schopf, P. S.: Ocean data assimilation using intermittent analyses and continuous model error correction, *Adv. Atmos. Sci.*, 19, 965–992, doi:10.1007/s00376-002-0059-z, 2002.
- Intergovernmental Panel on Climate Change (IPCC): Climate change 2013: The physical science basis, in *Contribution of Working Group I to the Fifth Assessment Report of the Intergovernmental Panel on Climate Change*, edited by Stocker, T. F., Qin, D., Plattner, G.-K., Tignor, M., Allen, S. K., Boschung, J., Nauels, A., Xia, Y., Bex, V., and Mdgley, P. M., p. 1535, Cambridge University Press, Cambridge, U.K.; New York, NY, USA, 2013.
- 335 Intergovernmental Panel on Climate Change (IPCC): Global warming of 1.5°C. An IPCC Special Report on the impacts of global warming of 1.5°C above pre-industrial levels and related global greenhouse gas emission pathways, in the context of strengthening the global response to the threat of climate change, sustainable development, and efforts to eradicate poverty, edited by Masson-Delmotte, V., et al., Cambridge University Press, Cambridge, U.K., 2018
- 340 Ishii, M., and Kimoto, M.: Reevaluation of historical ocean heat content variations with time-varying XBT and MBT depth bias corrections, *J. Oceanogr.*, 65, 287–299, doi:10.1007/s10872-009-0027-7, 2009.
- Ishii, M., Shouji A., Sugimoto, S., and Matsumoto, T.: Objective analyses of sea-surface temperature and marine meteorological variables for the 20th century using ICOADS and the Kobe Collection, *Int. J. Climatol.*, 25, 865–879, doi:10.1002/joc.1169, 2005.
- 345



- Ji, M., Behringer, D. W., and Leetmaa, A.: An improved coupled model for ENSO prediction and implications for ocean initialization. Part II: The coupled model, *Mon. Weather Rev.*, 126, 1022–1034, doi:10.1175/1520-0493(1998)126<1022:AICMFE>2.0.CO;2, 1998.
- 350 Jones, C. D., Collins, M., Cox, P. M., and Spall, S. A.: The carbon cycle response to ENSO: A coupled climate–carbon cycle model study, *J. Clim.*, 14, 4113–4129, doi:10.1175/1520-0442(2001)014<4113:TCCRTE>2.0.CO;2, 2001.
- Kalman, R. E.: A new approach to linear filtering and prediction problems, *Trans. ASME J. Basic Eng.*, 82, 35–45, 1960.
- Kalnay, E., Li, H., Miyoshi, T., Yang, S.-C., and Ballabrera-Poy, J.: 4-D-Var or ensemble Kalman filter?, *Tellus*, 59A, 758–773. doi:10.1111/j.1600-0870.2007.00261.x, 2007.
- 355 Kawamiya, M., Hajima, T., Tachiiri, K., and Yokohata, T.: Two decades of Earth system modeling, submitted to *Prog. Earth Planetary Sci.*, 2019.
- Keeling, C. D., and Revelle, R.: Effects of El Niño/Southern Oscillation on the atmospheric content of carbon dioxide, *Meteoritics*, 20, 437–450, 1985.
- Keenlyside, N. S., Latif, M., Jungclaus, J., Kornblueh, L., and Roeckner, E.: Advancing decadal-scale climate prediction in
360 the North Atlantic sector, *Nature*, 453, 84–88, doi:10.1038/nature06921, 2008.
- Kobayashi, S., Ota, Y., Harada, Y., Ebata, A., Moriya, M., Onoda, H., Onogi, K., Kamahori, H., Kobayashi, C., Endo, H., Miyaoka, K., and Takahashi, K.: The JRA-55 Reanalysis: General specifications and basic characteristics, *J. Meteorol. Soc. Japan*, 93(1), 5–48, doi:10.2151/jmsj.2015-001, 2015.
- Landschützer, P., Gruber, N., Bakker, D. C. E., and Schuster, U.: Recent variability of the global ocean carbon sink, *Glob.*
365 *Biogeochem. Cycles*, 28, 927–949, doi:10.1002/2014GB004853, 2014.
- Le Borgne, R., Feely, R. A., and Mackey, D. J.: Carbon fluxes in the equatorial Pacific: A synthesis of the JGOFS programme, *Deep-Sea Res. II*, 49, 2425–2442, doi:10.1016/S0967-0645(02)00043-7, 2002.
- Lengaigne, M., Hausmann, U., Madec, G., Menkes, C., Vialard, J., and Molines, J. M.: Mechanisms controlling warm water volume interannual variations in the equatorial Pacific: Diabatic versus adiabatic processes, *Clim. Dyn.*, 38, 1031–
370 1046, doi:10.1007/s00382-011-1051-z, 2012.
- Le Quéré, C., Raupach, M. R., Canadell, J. G., Marland, G., Bopp, L., Ciais, P., Conway, T. J., Doney, S. C., Feely, R. A., Foster, P., Friedlingstein, P., Gurney, K., Houghton, R. A., House, J. I., Hunginford, C., Levy, P. E., Lomas, M. R., Majkut, J., Metzl, N., Ometto, J. P., Peters, G. P., Prentice, I. C., Randerson, J. T., Running, S. W., Sarmiento, J. L., Schuster, U., Sitch, S., Takahashi, T., Viovy, N., van der Werf, G. R., and Woodward, F. I.: Trends in the sources
375 and sinks of carbon dioxide, *Nature Geosci.*, 2, 831–836, doi:10.1038/ngeo689, 2009.
- Le Quéré, C., Takahashi, T., Buitenhuis, E. T., Rödenbeck, C., and Sutherland, S. C.: Impact of climate change and variability on the global oceanic sink of CO₂, *Glob. Biogeochem. Cycles*, 24, GB4007, doi:10.1029/2009GB003599, 2010.
- Le Quéré, C. et al.: Global carbon budget 2016, *Earth Syst. Sci. Data*, 8, 605–649, doi:10.5194/essd-8-605-2016, 2016.



- 380 Li, G., and Xie, S.-P.: Tropical biases in CMIP5 multimodel ensemble: The excessive equatorial pacific cold tongue and double ITCZ problems, *J. Clim.*, 27, 1765–1780, doi:10.1175/JCLI-D-13-00337.1, 2014.
- Li, H., Ilyina, T., Müller, W. A., and Sienz, F.: Decadal predictions of the North Atlantic CO₂ uptake, *Nat. Commun.*, 7, 11076, doi:10.1038/ncomms11076, 2016.
- Li, H., Ilyina, T., Müller, W. A., and Landschützer, P.: Predicting the variable ocean carbon sink. *Sci. Adv.* 5, eaav6471, doi: 10.1126/sciadv.aav6471, 2019.
- 385 McKinley, G. A., Follows, M. J., and Marshall, J.: Mechanisms of air–sea CO₂ flux variability in the equatorial Pacific and the North Atlantic, *Glob. Biogeochem. Cycles*, 18, GB2011, doi:10.1029/2003GB002179, 2004.
- Meehl, G. A., Gent, P. R., Arblaster, J. M., Otto-Bliesner, B. L., Brady, E. C., and Craig, A.: Factors that affect the amplitude of El Niño in global coupled climate models, *Clim. Dyn.*, 17, 515–526, doi:10.1007/PL00007929, 2001.
- 390 Mochizuki, T., Ishii, M., Kimoto, M., Chikamoto, Y., Watanabe, M., Nozawa, T., Sakamoto, T. T., Shiogama, H., Awaji, T., Sugiura, N., Toyoda, T., Yasunaka, S., Tatebe, H., and Mori, M.: Pacific decadal oscillation hindcasts relevant to near-term climate prediction, *Proc. Nat. Acad. Sci. USA*, 107(5), 1833–1837, doi:10.1073/pnas.0906531107, 2010.
- Obata, A., and Kitamura, Y.: Interannual variability of the sea–air exchange of CO₂ from 1961 to 1998 simulated with a global ocean circulation-biogeochemistry model, *J. Geophys. Res.*, 108(C11), 3337, doi:10.1029/2001JC001088, 2003.
- 395 Park, G.-H., Wanninkhof, R., Doney, S. C., Takahashi, T., Lee, K., Feely, R. A., Sabine, C. L., Triñanes, J., and Lima, I.: Variability of global net sea–air CO₂ fluxes over the last three decades using empirical relationships, *Tellus B Chem. Phys. Meteorol.*, 62(5), 352–368, doi:10.1111/j.1600-0889.2010.00498.x, 2010.
- Park, J.-Y., Stock, C. A., Yang, X., Dunne, J. P., Rosati, A., John, J., and Zhang, S.: Modeling global ocean biogeochemistry with physical data assimilation: A pragmatic solution to the Equatorial instability, *J. Adv. Model. Earth Syst.*, 10, 891–906, doi:10.1002/2017MS001223, 2018.
- 400 Patra, P. K., Maksyutov, S., Ishizawa, M., Nakazawa, T., Takahashi, T., and Ukita, J.: Interannual and decadal changes in the sea–air CO₂ flux from atmospheric CO₂ inverse modeling, *Glob. Biogeochem. Cycles*, 19, GB4013, doi:10.1029/2004GB002257, 2005.
- 405 Pohlmann, H., Jungclaus, J. H., Köhl, A., Stammer, D., and Marotzke, J.: Initializing decadal climate predictions with the GECCO oceanic synthesis: Effects on the North Atlantic, *J. Clim.*, 22, 3926–3938, doi:10.1175/2009JCLI2535.1, 2009.
- Rödenbeck, C., Bakker, D. C. E., Metzl, N., Olsen, A., Sabine, C., Cassar, N., Reum, F., Keeling, R. F., and Heimann, M.: Interannual sea–air CO₂ flux variability from an observation-driven ocean mixed-layer scheme, *Biogeosciences*, 11, 4599–4613, doi:10.5194/bg-11-4599-2014, 2014.
- 410 Sabine, C. L., Feely, R. A., Gruber, N., Key, R. M., Lee, K., Bullister, J. L., Wanninkhof, R., Wong, C. S., Wallace, D. W. R., Tilbrook, B., Millero, F. J., Peng, T.-H., Kozyr, A., Ono, T., and Rios, A. F.: The oceanic sink for anthropogenic CO₂, *Science*, 305, 367–371, doi:10.1126/science.1097403, 2004.



- 415 Sasaki, Y.: Proposed inclusion of time variation terms, observational and theoretical, in numerical variational objective analysis, *J. Meteor. Soc. Japan*, 47, 115–124, 1969.
- Sasaki, Y.: Some basic formalisms in numerical variational analysis, *Mon. Wea. Rev.*, 98, 875–883, 1970.
- Smith, D. M., Cusack, S., Colman, A. W., Folland, C. K., Harris, G. R., and Murphy, J. M.: Improved surface temperature prediction for the coming decade from a global climate model, *Science*, 317, 796–799, doi:10.1126/science.1139540, 2007.
- 420 Sospedra-Alfonso, R., and Boer, G. J.: Assessing the impact of initialization on decadal prediction skill, *Geophys. Res. Lett.*, 47, e2019GL086361. doi:1029/2019GL086361, 2020.
- Sugiura, N., Awaji, T., Masuda, S., Toyoda, T., Igarashi, H., Ishikawa, Y., Ishii, M., and Kimoto, M.: Potential for decadal predictability in the North Pacific region, *Geophys. Res. Lett.*, 36, L20701, doi:10.1029/2009GL039787, 2009.
- Takahashi, T., Olafsson, J., Goddard, J. G., Chipman, D. W., and Sutherland, S. C.: Seasonal variation of CO₂ and nutrients
425 in the high-latitude surface oceans: A comparative study, *Glob. Biogeochem. Cycles*, 7(4), 843–878, doi:10.1029/93GB02263, 1993.
- Tatebe, H., Ishii, M., Mochizuki, T., Chikamoto, Y., Sakamoto, T. T., Komuro, Y., Mori, M., Yasunaka, S., Watanabe, M., Ogochi, K., Suzuki, T., Nishimura, T., and Kimoto, M.: The initialization of the MIROC climate models with hydrographic data assimilation for decadal prediction, *J. Meteorol. Soc. Japan*, 90A, 275–294,
430 doi:10.2151/jmsj.2012-A14, 2012.
- Taylor, K. E., Stouffer, R. J., and Meehl, G. A.: An overview of CMIP5 and the experiment design, *Bull. Amer. Meteorol. Soc.*, 93, 485–498, doi:10.1175/BAMS-D-11-00094.1, 2012.
- Tommasi, D. et al.: Managing living marine resources in a dynamic environment: The role of seasonal to decadal climate forecasts, *Prog. Oceanogr.*, 152, 15–49, doi:10.1016/j.pocean.2016.12.011, 2017a.
- 435 Tommasi, D., Stock, C. A., Alexander, M. A., Yang, X., Rosati, A., and Vecchi, G. A.: Multi-annual climate predictions for fisheries: An assessment of skill of sea surface temperature forecasts for large marine ecosystems, *Front. Mar. Sci.*, 4, 201, doi:10.3389/fmars.2017.00201, 2017b.
- Valsala, V., and Maksyutov, S.: Simulation and assimilation of global ocean pCO₂ and air–sea CO₂ fluxes using ship observations of surface ocean pCO₂ in a simplified biogeochemical offline model, *Tellus B Chem. Phys. Meteorol.*,
440 62B, 821–840, doi:10.1111/j.1600-0889.2010.00495.x, 2010.
- Valsala, V., Maksyutov, S., Telszewski, M., Nakaoka, S., Nojiri, Y., Ikeda, M., and Murtugudde, R.: Climate impacts on the structures of the North Pacific air–sea CO₂ flux variability, *Biogeosciences*, 9, 477–492, doi:10.5194/bg-9-477-2012, 2012.
- Wanninkhof, R.: Relationship between wind speed and gas exchange over the ocean, *J. Geophys. Res.*, 97(C5), 7373–7382,
445 doi:10.1029/92JC00188, 1992.
- Wanninkhof, R.: Relationship between wind speed and gas exchange over the ocean revisited, *Limnol. Oceanogr. Methods*, 12, 351–362, doi:10.4319/lom.2014.12.351, 2014.



- 450 Watanabe, M., Suzuki, T., O'ishi, R., Komuro, Y., Watanabe, S., Emori, S., Takemura, T., Chikira, M., Ogura, T., Sekiguchi, M., Takata, K., Yamazaki, D., Yokohata, T., Nozawa, T., Hasumi, H., Tatebe, H., and Kimoto, M.: Improved climate simulation by MIROC5: Mean states, variability, and climate sensitivity, *J. Clim.*, 23, 6312–6335, doi:10.1175/2010JCLI3679.1, 2010.
- Watanabe, M., Chikira, M., Imada, Y., and Kimoto, M.: Convective control of ENSO simulated in MIROC, *J. Clim.*, 24, 543–562, doi:10.1175/2010JCLI3878.1, 2011.
- 455 Watanabe, S., Hajima, T., Sudo, K., Nagashima, T., Takemura, T., Okajima, H., Nozawa, T., Kawase, H., Abe, M., Yokohata, T., Ise, T., Sato, H., Kato, E., Takata, K., Emori, S., and Kawamiya, M.: MIROC-ESM 2010: Model description and basic results of CMIP5-20c3m experiments, *Geosci. Model Dev.*, 4, 845–872, doi:10.5194/gmd-4-845-2011, 2011.
- Weiss, R.: Carbon dioxide in water and seawater: The solubility of a non-ideal gas, *Mar. Chem.*, 2, 203–215, doi:10.1016/0304-4203(74)90015-2, 1974.
- 460 Yang, X., Rosati, A., Zhang, S., Delworth, T. L., Gudgel, R. G., Zhang, R., Vecchi, G., Anderson, W., Chang, Y.-S., DelSole, T., Dixon, K., Msadek, R., Stern, W. F., Wittenberg, A., and Zeng, F.: A predictable AMO-like pattern in the GFDL fully coupled ensemble initialization and decadal forecasting system, *J. Clim.*, 26, 650–661, doi:10.1175/JCLI-D-12-00231.1, 2013.

465

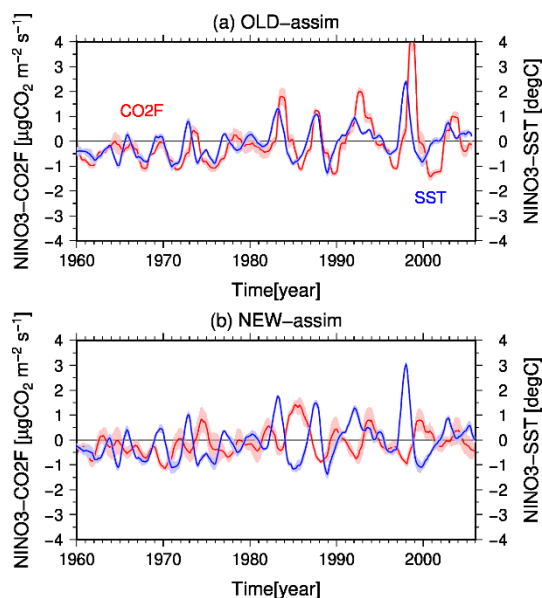
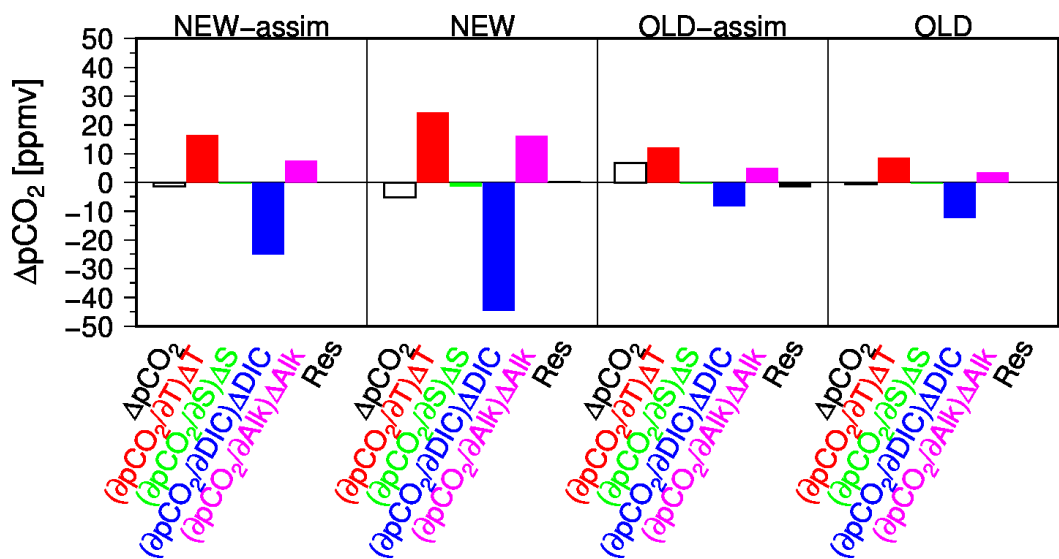


Figure 1. Time variations of the ensemble mean sea surface temperature (SST; blue line) and air–sea CO₂ flux (CO₂F, positive upward; red line) in the Niño3 region (5°S–5°N, 90°–150°W) simulated with (a) OLD-assim and (b) NEW-assim. Values plotted are the one-year running mean and shading shows the standard deviation.

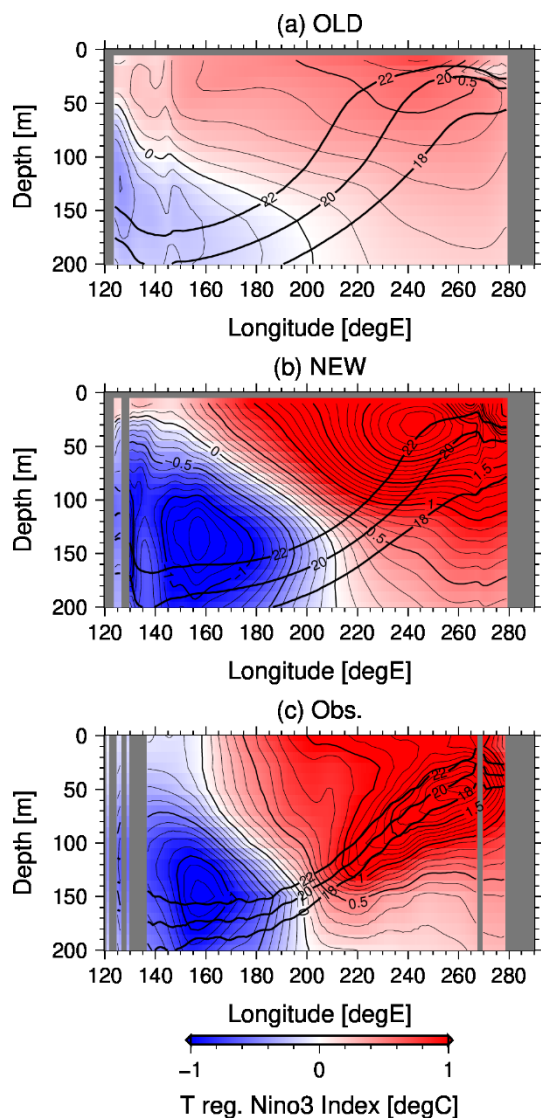


470

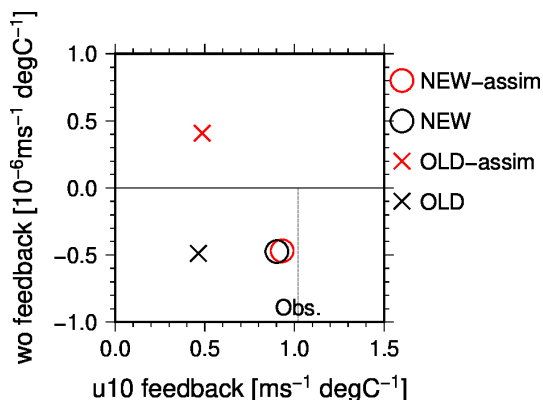


475

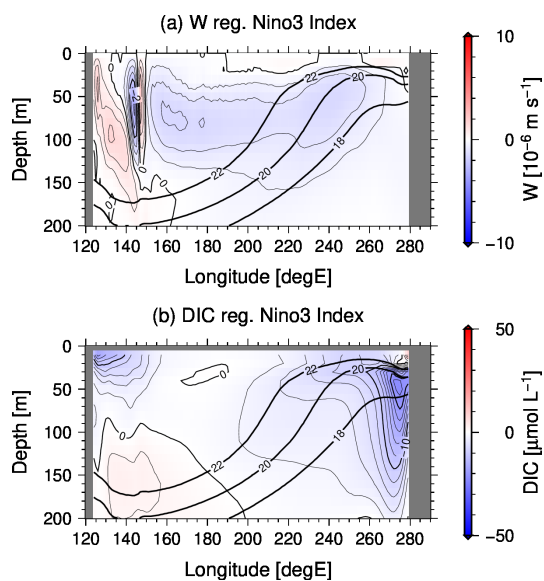
Figure 2. Each term in Eq. (3) evaluated in NEW-assim, NEW, OLD-assim, and OLD. ΔX ($X = pCO_2, T, S, DIC, \text{ or } Alk$) in Eq. (3) is estimated as X regressed onto NINO3-SST, and $\partial pCO_2/\partial X$ is estimated with the climatological annual mean $T, S, DIC, \text{ and } Alk$ at the sea surface within the Niño3 region in each model.



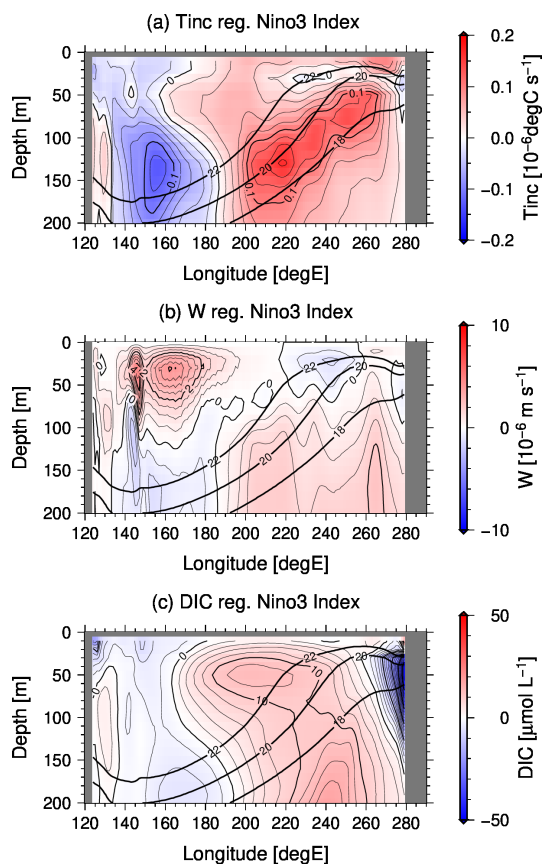
480 **Figure 3.** Cross sections along the Equator of monthly water temperature anomaly in (a) OLD, (b) NEW, and (c) derived from the observational dataset by Ishii and Kimoto (2009), each regressed onto NINO3-SST. Contour interval is 0.1 °C. Solid lines show the climatological annual mean depths of the 18, 20, and 22 °C isotherms.



485 **Figure 4.** Relationship between the wind (u10) feedback and the vertical velocity (wo) feedback in OLD (black cross), OLD-assim (red cross), NEW (black circle), and NEW-assim (red circle). Wind feedback (vertical velocity feedback) was computed as the regression of NINO4-U10 over NINO3-SST ($\text{m s}^{-1} \text{ } ^\circ\text{C}^{-1}$) (regression of NINO3-WO over NINO3-SST ($\text{m s}^{-1} \text{ } ^\circ\text{C}^{-1}$)). Thin dashed line shows wind feedback evaluated from the JRA55 reanalysis wind dataset (Kobayashi et al., 2015) and the COBESST2 dataset (Ishii et al., 2005; Hirahara et al., 2014).



490 **Figure 5.** Cross sections along the Equator of monthly (a) upward velocity and (b) DIC concentration anomalies with OLD, each regressed onto NINO3-SST. Contour interval is $0.5 \times 10^{-6} \text{ m s}^{-1}$ in (a) and $2 \text{ } \mu\text{mol L}^{-1}$ in (b).



495 **Figure 6. Cross sections along the Equator of (a) water temperature increment, (b) upward velocity, and (c) DIC concentration with OLD-assim each regressed onto NINO3-SST. Contour interval is $0.02 \times 10^{-6} \text{ }^{\circ}\text{C s}^{-1}$ in (a), $0.5 \times 10^{-6} \text{ m s}^{-1}$ in (b), and $2 \mu\text{mol L}^{-1}$ in (c).**

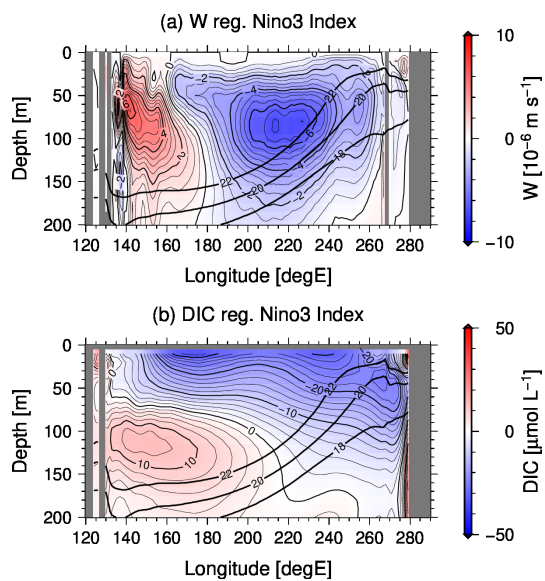


Figure 7. As Figure 5 but for NEW.

500

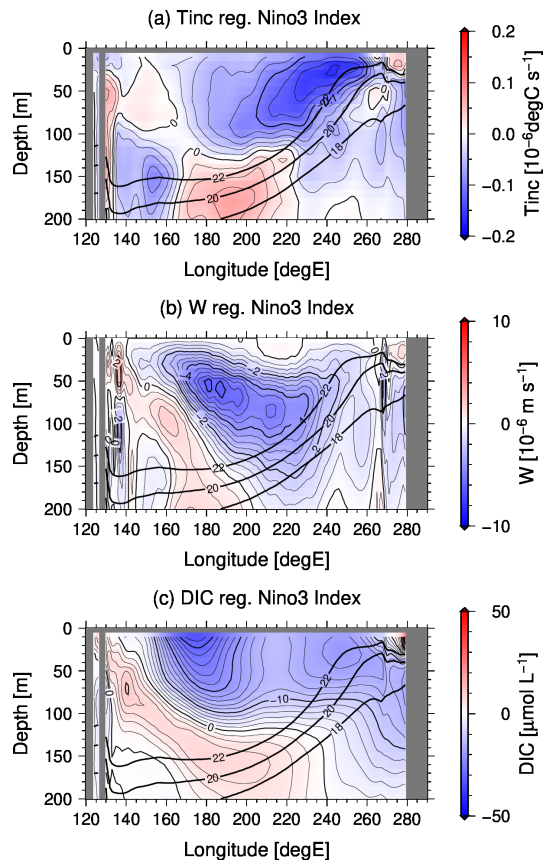


Figure 8. As Figure 6 but for NEW-assim.